Food Research International 242 (2026) 119803

Contents lists available at ScienceDirect

Food Research International

journal homepage: www.elsevier.com/locate/foodres

Influence of extraction method on structural, rheological, and nutritional characterization of peach palm (*Bactris gasipaes*) fruits pulp and peel oils

Hermanny Matos Silva Sousa [a,*], Rômulo Alves Morais [b], Federico Basso [c], Roberta Pratolino [c], Luana Regina Pereira Alves [b], Gabriela Fonsêca Leal [a], Monica Anese [c], Fabiana Queiroz [a], Paulo Peres de Sá Peixoto [d], Sonia Calligaris [c], Glêndara Aparecida de Souza Martins [b]

[a] Graduate Program in Food Science, Federal University of Lavras, Lavras, MG 37200-900, Brazil
[b] Laboratory of Kinetics and Process Modeling (LaCiMP), Federal University of Tocantins, Palmas, TO 77001-090, Brazil
[c] Department of Agricultural, Food, Environmental and Animal Sciences, University of Udine, Via Sondrio 2/A, 33100 Udine, Italy
[d] UMET CNRS Laboratory, INRAE, UMR 8207-UMET-PIHM, Lille University, 59652 Villeneuve-d'Ascq, France - UMET - Unité Matériaux et Transformations, équipe Processus aux Interfaces et Hygiène des Matériaux (PIHM), F-59000 Lille, France

ARTICLE INFO

Keywords:
Amazonian palm oil
Fruit peel valorization
Lipophilic bioactives
Lipid structure
Rheology
Triacylglycerols

ABSTRACT

Peach palm (*Bactris gasipaes*) is a promising tropical resource, yet its fruit oils remain poorly understood from both chemical and structure–function perspectives. This study investigated how the fruit fraction (pulp and peel) and the extraction protocol modulated the chemical composition, multiscale organization, and technological functionality of peach palm oils. Oils obtained from pulp and peel using conventional isooctane- and ethanol-based protocols were evaluated through an integrated chemical, thermal, structural, and rheological approach. The oils were characterized for fatty acid profiles, lipid quality indices, predicted triacylglycerol composition, carotenoids, thermal transitions by differential scanning calorimetry, crystal morphology by polarized light microscopy, supramolecular and crystalline organization by small- and wide-angle X-ray scattering/diffraction, and oscillatory rheology at 20 °C. Rheological measurements were performed only on samples that exhibited structured behavior at room temperature, namely, pulp oil obtained using the isooctane-based protocol and peel oil obtained using the ethanol-based protocol. All oils were rich in oleic acid, reaching up to 63.98%, and displayed favorable lipid quality indices, including low atherogenicity and thrombogenicity indices. The predicted triacylglycerol profiles suggested a predominance of mixed saturated–unsaturated species, especially palmitoyl-dioleoyl-glycerol, a monounsaturated–dipalmitoyl–oleoyl–glycerol, followed by trioleoyl-glycerol and dipalmitoyl-oleoyl-glycerol. Carotenoids, particularly β-carotene and lycopene, were detected at measurable levels, with protocol- and fraction-dependent differences; lycopene was not detected in pulp oil extracted with ethanol. Differential scanning calorimetry revealed complex crystallization and melting behavior, with room-temperature structuring that depended on the combined effects of the extraction protocol and the fruit fraction. Pulp oil obtained via the isooctane-based protocol and peel oil obtained via the ethanol-based protocol exhibited melting/crystallization events extending to approximately 20 °C and behaved as semi-solid systems. Microscopy, scattering/diffraction, and rheology supported the development of interconnected crystal networks and organized lipid domains only in these structured oils. Overall, extraction conditions and tissue fraction jointly governed lipid organization and functionality, supporting the use of peach palm pulp and peel oils as potential ingredients for future food and cosmetic formulation studies.

1. Introduction

Vegetable oils play a central role in human nutrition, acting as major energy sources, supplying essential fatty acids, and serving as carriers for lipophilic bioactives and micronutrients (Polmann et al., 2024; Gualberto et al., 2025; Morais et al., 2022, Tian et al., 2023). Beyond

* Corresponding author.
E-mail address: hermanny_97@hotmail.com (H.M.S. Sousa).

https://doi.org/10.1016/j.foodres.2026.119803
Received 10 April 2026; Received in revised form 1 June 2026; Accepted 20 June 2026
Available online 22 June 2026

their dietary relevance, vegetable oils are fundamental techno-functional ingredients in food systems, where their fatty acid profile and triacylglycerol (TAG) distribution govern crystallization, polymorphic behavior, and the formation of fat crystal networks that ultimately control texture, spreadability, mouthfeel, and process stability. Minor constituents, such as carotenoids, tocopherols, and phytosterols, further contribute to nutritional value and may influence physical behavior by interacting with lipid assemblies and affecting phase organization (Ibiapina et al., 2021). Therefore, understanding oil composition together with multiscale structural organization is increasingly necessary to rationally design products with tailored functionality (e.g., structured emulsions, semi-solid fats, and fat-based matrices) while meeting nutritional expectations.

In the current scenario, the demand for novel and sustainable lipid sources has intensified due to the need to diversify the global oil supply chain, reduce dependence on a limited number of commodity oils, and mitigate the environmental and socio-economic impacts associated with conventional oilseed cultivation, such as land use change, deforestation, and high agricultural inputs (Tian et al., 2023). In parallel, economic drivers, including price volatility, supply insecurity, and the growing industrial demand for fats with specific functionality, have further accelerated the search for alternative oils capable of delivering consistent structure and performance in foods. In this context, there is increasing interest in valorizing lipid sources from underexplored regions, particularly Amazonia, that can be obtained from non-intensive systems, agroforestry practices, or extractive chains, contributing to biodiversity conservation and local economic development is essential to define their potential as structured lipids and as carriers of lipophilic bioactives for food and cosmetic applications. (Montoro-Alonso et al., 2025).

Peach palm (*Bactris gasipaes*), an Amazonian species in the family Arecaceae, is a promising source of edible oils. Its fruits present significant lipid contents (approximately 7.5% in the peel and 6.5% in the pulp), and the extracted oils are characterized by a **predominance of unsaturated fatty acids**, particularly **oleic acids (54%)**, resulting in a relevant proportion of **polyunsaturated fatty acids**, which are nutritionally desirable and technologically relevant for food and cosmetic applications (Ibiapina et al., 2021; Sousa et al., 2025). Moreover, notable concentrations of natural pigments, especially carotenoids (around 34.74 mg 100 g^{-1} in the peel), can be co-extracted with the oil, conferring it a remarkable health-promoting capacity (Miranda et al., 2024; Sousa et al., 2025). Yet, despite its chemical characteristics, peach palm fruit remains underexploited for lipid valorization, as its industrial use is still largely focused on fresh consumption and starch-rich products, with lipid-rich fractions often overlooked. The integrated use of peach palm fruit fractions, particularly the peel, which is commonly underutilized during processing, offers an opportunity to obtain value-added lipid ingredients. This approach may contribute to resource efficiency and circular bioeconomy strategies by expanding the use of Amazonian fruit fractions that are currently undervalued. However, it is important to distinguish the sustainability potential associated with biomass valorization from the environmental limitations of the extraction procedures used to recover lipids. In the present study, the oils were obtained using conventional solvent-based extraction protocols, including isooctane- and ethanol-based protocols.

The extraction process used to separate the lipid fraction plays a decisive role in the yield and characteristics of vegetable oils. Traditional non-polar solvents, such as isooctane and n-hexane, are effective for solubilizing non-polar lipids, but their toxicity, fossil-based origin, volatility, and environmental concerns have spurred the search for safer, more sustainable alternatives (Freitas et al., 2024; Morais et al., 2025). Ethanol, in contrast, is generally regarded as a more environmentally acceptable solvent due to its lower toxicity, biodegradability, and potential renewable origin, although its sustainability also depends on source, recovery, and process conditions (Gomaa et al., 2022; Menezes Silva et al., 2023). Therefore, the comparison between the isooctane-based and ethanol-based protocols in this study should not be interpreted as a comparison between unsustainable and fully green extraction methods, but rather as an evaluation of two conventional solvent-based protocols with distinct polarity and operating conditions. Furthermore, the technological performance and functional properties of oils are closely related to their molecular organization and their thermal and rheological properties. The **fatty acid composition of triacylglycerols**, particularly the proportion of monounsaturated fatty acids, together with **minor lipid components, such as carotenoids**, can influence triacylglycerol crystallization pathways and affect polymorphism, viscosity, and melting behavior (Sivakanthan et al., 2022). These attributes are essential for predicting product stability, texture, and performance in food formulations.

Despite the chemical and functional potential of peach palm fruit oils, limited information is available on the multiscale relationships between their composition, structural organization, and technological behavior. In this study, two conventional solvent-based extraction protocols were compared: an isooctane-based protocol and an ethanol-based protocol. These protocols differed not only in solvent polarity but also in extraction time, temperature, mechanical treatment, and separation steps. Therefore, the observed differences were interpreted as effects of the overall extraction protocol rather than as the isolated effect of solvent polarity. Based on this premise, the aim of the present study was to investigate how fruit fraction and extraction protocol influence the chemical profile, lipid quality indices, estimated triacylglycerol composition, carotenoid content, differential scanning calorimetry, polarized light microscopy, small- and wide-angle X-ray scattering, and rheological properties of peach palm pulp and peel oils. The novelty of this study does not lie in the extraction procedures themselves, which are conventional solvent-based protocols, but in the integrative characterization of peach palm oils using complementary chemical, thermal, structural, and rheological techniques, providing new insights into the structure–function behavior of this underexplored Amazonian lipid source.

2. Materials and methods

2.1. Chemicals and reagents

Isooctane (≥99.0%) and pentane (≥99.0%) were purchased from Sigma Aldrich (Milan, Italy). Absolute ethanol was purchased from Sigma Aldrich (São Paulo, Brazil). The fatty acid standards used were 20, including saturated (lauric, myristic, pentadecanoic, palmitic, heptadecanoic, stearic, arachidic, heinecosanoic, behenic, tricosanoic, and lignoceric acids), monounsaturated (palmitoleic acid *n*7 and *n*9, heptadecenoic, oleic, and eicosenoic acids), and polyunsaturated (linoleic, α-linolenic, eicosadienoic, and *cis*-13,16-docasadienoic acids) purchased from Sigma Aldrich (Milan, Italy).

2.2. Sample

Peach palm fruits (*Bactris gasipaes*) were obtained in the state of Pará, Brazil (latitude 08°01′43″ S, longitude 50°01′53″ W), located in the Amazon region. The fruits used in this study corresponded to ripe Amazonian peach palm fruits characterized by a red-orange peel and yellow-orange pulp, as shown in Fig. 1. The fruits were washed and sanitized with 100 ppm sodium hypochlorite. They were then manually separated into peel, pulp, and seed fractions. The peel and pulp fractions were dried in an air-circulation oven (Solab, SL102, Brazil) at 50 °C until a constant weight was reached. The dried pulp and peel were ground in a knife mill to a standard particle size of 1.00 mm (Tecnal, TE-650, Brazil), yielding peach palm pulp and peel flours. The flours were vacuum-packed and stored at −20 °C until analysis.

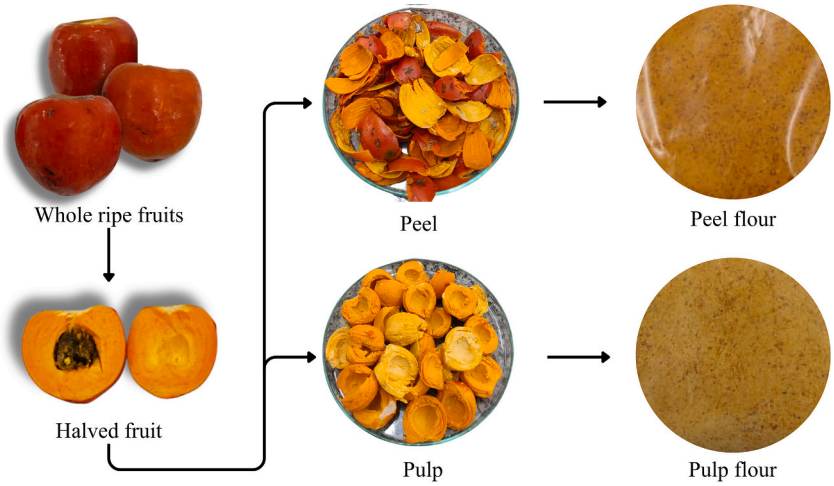

Fig. 1. Representative visual documentation of the peach palm (*Bactris gasipaes*) fruits used in this study, including whole ripe fruits, halved fruit, separated peel and pulp fractions, and the corresponding peel and pulp flours obtained after drying and milling.

2.3. Oil extraction protocols

Oils were extracted from peach palm pulp (PU) and peel (PE) flours using two extraction protocols, which differed in both solvent polarity and operating conditions. For the non-polar protocol, 50 g of PU or PE flour was mixed with 500 mL of isooctane analytical grade (A.G) (solid-to-solvent ratio 1:10, *w/v*) in glass bottles and homogenized using an Ultra-Turrax (T18, IKA) at 10,000 rpm for 15 min. The mixtures were filtered through quantitative filter paper, and isooctane was removed using a rotary evaporator (Heidolph, Germany) coupled to a vacuum pump (Vacuum Pump V-700, Büchi, Switzerland), with the water bath maintained at 60 °C under vacuum. After solvent removal, the recovered oils were briefly re-dissolved in a small volume of analytical-grade pentane to facilitate quantitative transfer from the evaporation flask to amber vials and to minimize sample losses during handling. Pentane was selected for its high volatility and completely evaporated under a gentle nitrogen stream immediately after transfer. The vials were flushed with nitrogen and stored at −20 °C until analysis. Resulting in isooctane-based protocol pulp (PU-ISO) and isooctane-based protocol peel (PE-ISO) treatments. This step was used only for sample recovery and transfer and was not intended as an additional extraction step. All manipulations were performed as rapidly as possible and protected from direct light to minimize carotenoid degradation.

For the polar protocol, 50 g of PU or PE flour was mixed with 500 mL of ethanol (A.G) (1:10, *w/v*), incubated at 50 °C for 4 h under constant agitation, and then filtered and centrifuged at 17,000 rpm at 4 °C to separate the solvent from the oil. The headspace of the vials containing the extracted oils was flushed with nitrogen, and samples were stored at −20 °C until analysis. Resulting in ethanol-based extraction protocol pulp (PU-ET) and ethanol-based extraction protocol peel (PE-ET) treatments. Extraction yield was determined gravimetrically as the ratio of the mass of oil recovered after solvent removal to the initial dry mass of the flour used, expressed as a percentage (%).

2.4. Chemical characterization

2.4.1. Fatty acid composition

The reference procedure was performed according to the method described in the International Olive Council (IOC) (2017) method T20–33-rev-1. Aliquots of 0.1 g of oil were mixed with 2 mL of *n*-heptane and 0.2 mL of 2 N methanolic KOH solution, shaken vigorously for 30 s, then left to stratify. The upper phase containing fatty acid methyl esters was analyzed (injection volume 1 μL). The analysis was carried out on a Gas Chromatograph (GC) Trace 1300 (Thermo Fisher Scientific) coupled to an FID detector. The chromatographic conditions were as follows: capillary column of fused silica SP-2330 (Supelco, USA), 60 m long with 0.32 mm internal diameter, filled with 0.2 μm polyethylene glycol. The operating conditions were: Split injection, 50:1 ratio; Column temperature: 100 °C for 5 min, programmed to 200 °C at 5 °C min^{-1}, then to 240 °C at 3 °C min^{-1}, held for 8 min (total run time 40 min). Helium was the carrier gas at a constant pressure of 130 kPa. Injector and detector temperatures are both 250 °C. Fatty acid standards were used to identify compounds by comparing the retention times of detected peaks with those of the corresponding reference standards. No internal standard or response correction factors were applied for quantitative calibration. Therefore, the fatty acid results were expressed as relative composition, calculated from the percentage of each fatty acid methyl ester's peak area relative to the total identified peak area.

2.4.2. Nutritional and health indices

Based on the fatty acid composition of PU and PE extracted oils, the nutritional value (NVI), atherogenicity (AI), thrombogenicity (TI) and hypo- and hypercholesterolemic (HH) were calculated (Chen & Liu, 2020) according to the following equations:

$$NVI = \frac{(C18:0 + C18:1)}{(C16:0)} \quad (1)$$

$$AI = \frac{C12:0 + 4\,x\,C14:0 + C16:0}{\sum MUFA + \sum FA\omega6 + \sum FA\omega3} \quad (2)$$

$$TI = \frac{C14:0 + C16:0 + C18:0}{(0.5\,x \sum MUFA\,) + (0.5\,x \sum FA\omega6) + (0.5\,x \sum FA\omega3)} \quad (3)$$

$$HH = \frac{(C18:1 + \sum PUFA)}{(C12:0 + C14:00 + C16:00)} \quad (4)$$

Where C12:0, C14:0, C16:0, C18:0, and C18:1 represent the relative mass percentages of lauric, myristic, palmitic, stearic, and oleic acids, respectively; MUFA refers to the relative mass percentage of monounsaturated fatty acids; FA ω6 and FA ω3 indicate the relative mass percentages of omega-6 and omega-3 fatty acids, respectively; PUFA refers to the relative mass percentage of polyunsaturated fatty acids.

2.4.3. Estimation of triacylglycerol composition

The composition of triacylglycerols (TAG) was estimated using the *PrOleos* software, as reported by Antoniosi Filho et al. (1995). The algorithm estimates the triacylglycerol content based on the *1,3-random-2-random* distribution hypothesis, which predicts the molar percentage of triacylglycerols in vegetable oils. This method utilizes a random

distribution model (without preference for the *sn*-1, sn-2, or sn-3 positions) of free fatty acids on the glycerol backbone, using the sample's fatty acid composition as input data.

2.4.4. Determination of β-carotene and lycopene by HPLC

β-Carotene and lycopene extraction was performed under subdued light, and a nitrogen atmosphere according to the method proposed by Bot et al. (2018), with minor modifications to the extraction phase solely. Aliquots of 200 μL of PU-ET, PU-ISO, PE-ET, and PE-ISO of oil melted at 40 °C were diluted in 2.0 mL of solvent mixture methanol and MTBE (50:50, *v*/v) and filtered through a 0.20 μm membrane filter before HPLC analysis. Chromatographic separation was carried out based on the method described by Sadler et al. (1990) and adapted Bot et al. (2018). Analyses were performed at 25 °C using a LC 4000 (Jasco Europe, Cremella, Italy) HPLC equipped with a YMC C30 column. The mobile phase, freshly prepared, consisted of two eluents: eluent A, composed of methanol and MTBE (90:10, v/v), and eluent B, composed of the same mixture at different ratio (10:90, v/v), both containing 0.1% (*w/v*) BHT. Elution was performed at a flow rate of 1.0 mL/min. Detection was carried out using a diode-array detector at 450 nm for β-carotene and 470 nm for lycopene. Carotenoids were quantified (reported average recovery of 99.3 and 99.6% for β-Carotene and lycopene, respectively) based on external calibration curves, considering for both compounds the linear range 1.25–10.0 μg/mL (equation for lycopene: y = 178,135×-26,373, equation for β-carotene: y = 341,542×-242,497; both calibration curves with $R^2 = 0.99$). Concentrations obtained from the chromatograms were corrected for the total dilution factor applied during sample preparation. All analyses were performed in duplicate, and data processing was carried out using STAR software version 5.3 (Varian).

2.5. Physical properties

2.5.1. Differential scanning calorimetry (DSC)

To perform calorimetric analyses, aliquots of each sample (~5 mg) were accurately weighed into 40 μL aluminum pans and sealed (Mettler-Toledo, Greifensee, Switzerland). The pans were then placed in the sensor cell of a DSC 3 StarE® System (Mettler-Toledo) and subjected to the following temperature ramp: 20 °C for 3 min; 20 to 80 °C at 5 °C min^{-1}; 80 °C for 3 min; 80 to −50 °C at −5 °C min^{-1}; −50 °C for 3 min; −50 to 80 °C at 5 °C min^{-1}. Normalized heat flow (W g^{-1}) was recorded using an empty pan as reference, and the entire analysis was performed under gentle nitrogen flow to limit sample oxidation. Peak temperatures and transition enthalpies were calculated from the obtained thermograms by using the STARe program ver. 16.10 (Mettler-Toledo).

2.5.2. Synchrotron X-ray diffractometry

Small-angle X-ray scattering (SAXS) and wide-angle X-ray scattering (XRD) analyses were performed at 20 °C at the SOLEIL synchrotron light facility in Saint-Aubin, France, using the SWING beamline with photon energies of approximately 12 keV (SAXS) and 16 keV (XRD). Four peach palm oil samples (PU-ET, PU-ISO, PE-ET, and PE-ISO) were evaluated in glass capillaries. The scattering intensity was recorded by a detector positioned at distances of approximately 0.5 m and 6.5 m from the sample, allowing data acquisition over a scattering-vector q range of 1.5 × 10^{-3} to 1.4 × 10^{-1} $Å^{-1}$. For each sample, data were initially collected with a short exposure time (~0.2 s) to minimize potential radiation damage and to avoid artifacts in the low-q region. Subsequent recordings were made with longer exposure times (~15 s) using a wider light beam to improve the signal-to-noise ratio at high *q* values. The intensities obtained at both exposure times were radially processed and combined into a single I(*q*) scattering curve, discarding segments with evidence of radiation-induced degradation. The solvent (ultra-pure water) scattering intensity was recorded under the same conditions and subtracted from the data for each sample, resulting in the corrected I(*q*) intensity (Nogueira et al., 2023). For data interpretation, Porod's Law was applied in the high-q region to analyze interfaces between domains with contrasting electron densities. Additionally, the Guinier Equation was used in the low-*q* region to estimate the radius of gyration (Rg) of the dispersed particles in the oils (Chen et al., 2022). The curve fitting of I(q) was performed in the Guinier regime, where the equation $I(q) = I(0)\exp\left(-q^2R_g^2/3\right)$ was applied to determine the radius of gyration. This approach enabled evaluation of the structural and supramolecular properties of the different lipid samples, depending on the solvent and the portion of the fruit used for extraction.

2.5.3. Rheological analysis

The rheological properties of the oils were assessed using a controlled-stress rheometer (Haake Rheostress 6000, Thermo Scientific, Karlsruhe, Germany). A plate-plate geometry (35 mm, 1 mm gap) was used. To determine the linear viscoelastic region, amplitude sweep tests were performed by increasing oscillatory stress from 0.1 to 100 Pa at a frequency of 1 Hz. The linear viscoelastic domain was identified at 20 °C for each sample as the stress domain in which G′ remained constant, with a maximum deviation lower than 5% from the initial value. Frequency sweep tests were performed by increasing oscillatory frequency from 0.1 to 10 Hz, applying a fixed stress value included in the linear viscoelastic region at 20 °C. Samples were maintained at room temperature (20 °C) for 24 h before analysis and, after being placed on the rheometer geometry, they were allowed to equilibrate for 5 min to ensure relaxation of internal stress. Measurements were performed in triplicate.

2.6. Polarized light microscope (PLM)

The samples were prepared by pouring a small amount of oil onto a glass microscope slide and then covering it with a coverslip. Then, gentle pressure was applied to ensure adequate thickness for measurement. The samples were preheated to 60 °C for 10 min to erase the crystal memory, then cooled at 5 °C min^{-1} to 20 °C using a water-cooling system attached to the microscope. Images were captured at 40× magnification using a microscope (Leica Microsystems, Wetzlar, Germany), operated by Leica Suite Las EZ software (Leica Microsystems, Heerbrugg, Switzerland), and saved in JPEG format.

2.7. Statistical analysis

The results were expressed as mean ± standard deviation. Measurements were performed in duplicate or triplicate, as indicated in the corresponding tables and figure captions. Data were analyzed using analysis of variance (ANOVA) at a 5% significance level ($p < 0.05$) using Statistica 10.0 software (StatSoft Inc., Tulsa, OK, USA). Prior to parametric comparisons, data were checked for normality and homogeneity of variances. When the homogeneity assumption was met, differences among means were assessed by ANOVA followed by Tukey's test. When variances were not homogeneous, Welch's ANOVA was applied. Synchrotron SAXS and XRD data were analyzed using the SasView software (*SasView*-6.1.1).

3. Results and discussion

3.1. Chemical characterization

Extraction yield was significantly affected by the **extraction protocol** ($p < 0.05$), with the ethanol-based protocol providing higher yields than the isooctane-based protocol for both pulp and peel oils (Table 1). Moreover, yields were slightly higher for pulp oils than for peel oils. **No significant protocol × fraction interaction was detected, indicating that the increase in yield observed when transitioning from the isooctane-based to the ethanol-based protocol was comparable for both pulp and peel oils.** The fatty acid

Table 1
Relative fatty acid composition and health indices of peach palm pulp and peel oils.

Analysis	PU-ISO	PU-ET	PE-ISO	PE-ET
Yield (%)	15 ± 0.1^{c}	20 ± 0.17^{a}	13 ± 0.12^{d}	18 ± 0.23^{b}
Fatty acid (%)				
C12:0 - Lauric acid	0.05 ± 0.01^{a}	0.01 ± 0.00^{a}	0.02 ± 0.00^{a}	0.02 ± 0.00^{a}
C14:0 - Myristic acid	0.15 ± 0.01^{a}	0.07 ± 0.01^{b}	0.11 ± 0.00^{a}	0.08 ± 0.01^{b}
C15:0 - Pentadecanoic acid	0.04 ± 0.00^{a}	0.04 ± 0.00^{a}	0.06 ± 0.00^{a}	0.06 ± 0.00^{a}
C16:0 - Palmitic acid	17.96 ± 0.1^{c}	33.92 ± 0.25^{a}	30.44 ± 0.41^{b}	34.05 ± 0.20^{a}
C16:1 ω9 - Palmitoleic acid	0.20 ± 0.29^{a}	0.49 ± 0.20^{a}	0.06 ± 0.00^{b}	0.07 ± 0.00^{b}
C16:1 ω7 - Palmitoleic acid	4.70 ± 0.25^{a}	3.96 ± 0.01^{bc}	4.34 ± 0.20^{ab}	3.80 ± 0.01^{c}
C17:0 - Heptadecanoic acid	0.07 ± 0.01^{a}	0.05 ± 0.05^{a}	0.06 ± 0.00^{a}	0.06 ± 0.00^{a}
C17:1 ω8- Heptadecenoic acid	0.05 ± 0.00^{a}	0.04 ± 0.00^{a}	0.05 ± 0.01^{a}	0.05 ± 0.00^{a}
C18:0 - Stearic acid	1.29 ± 0.10^{c}	1.55 ± 0.11^{a}	1.34 ± 0.01^{b}	1.47 ± 0.22^{ab}
C18:1 ω9 - Oleic acid	63.98 ± 0.23^{a}	53.06 ± 0.37^{b}	53.22 ± 0.06^{b}	51.80 ± 0.51^{b}
C18:2 ω6 - Linoleic acid	7.64 ± 0.01^{a}	5.36 ± 0.02^{c}	7.79 ± 0.05^{a}	6.18 ± 0.03^{b}
C20:0 - Arachidic acid	0.18 ± 0.00^{a}	0.13 ± 0.00^{b}	0.18 ± 0.01^{a}	0.18 ± 0.00^{a}
C18:3 ω3 - a-Linolenic acid	3.14 ± 0.02^{a}	1.18 ± 0.02^{c}	2.03 ± 0.02^{b}	1.91 ± 0.28^{b}
C20:1 ω9 - Eicosenoic acid	0.13 ± 0.00^{a}	0.06 ± 0.00^{b}	0.10 ± 0.02^{a}	0.08 ± 0.00^{ab}
C21:0 - Heinecosanoic acid	0.01 ± 0.00^{a}	0.01 ± 0.00^{a}	0.01 ± 0.00^{a}	0.01 ± 0.00^{a}
C20:2 - Eicosadienoic acid	ND	ND	ND	ND
C22:0 - Behenic acid	0.40 ± 0.00^{a}	0.04 ± 0.01^{b}	0.08 ± 0.03^{b}	0.04 ± 0.01^{b}
C24:0 - Lignoceric acid	ND	0.03 ± 0.00^{b}	0.08 ± 0.00^{a}	0.08 ± 0.00^{a}
Saturated (SFA)	20.16 ± 1.33^{c}	35.83 ± 0.74^{a}	32.36 ± 0.19^{b}	36.09 ± 0.44^{a}
Monounsaturated (MUFA)	69.06 ± 0.52^{a}	57.61 ± 0.12^{b}	57.78 ± 0.94^{b}	55.79 ± 0.38^{c}
Polyunsaturated (PUFA)	10.78 ± 0.11^{a}	6.57 ± 0.56^{c}	9.86 ± 0.65^{a}	8.13 ± 0.10^{b}
Health indices				
Nutritional value index (NVI)	3.62	1.61	1.79	1.64
Atherogenic index (AI)	0.23	0.53	0.46	0.51
Thrombogenic index (TI)	0.39	0.99	0.81	0.91
Hypocholesterolemic/ hypercholesterolemic (H/H)	4.14	1.76	2.06	1.84

Data are expressed as mean ± standard deviation ($n = 2$). Fatty acid values correspond to relative peak area percentages of identified fatty acid methyl esters. Equal letters on the same line show no significant difference (Tukey's test and *t*-test, $p < 0.05$). ND: not detected.

composition of the extracted oils is also reported in Table 1. Twenty fatty acids were identified in the analyzed peach palm oils, with wide variation between the pulp and peel samples, and additional variations were observed between the extraction protocols. The results showed that the samples had a predominance of monounsaturated fatty acids (MUFAs), followed by saturated fatty acids (SFA) and polyunsaturated fatty acids (PUFAs), as shown in Table 1. This distribution is typical of tropical oils from fruits of the *Arecaceae* family (Gualberto et al., 2025; Ibiapina et al., 2021).

Palmitic acid was the predominant SFA, ranging from 17.96 to 34.05%, which was comparable to the value reported for peach palm pulp oil (35.81%) by Sousa et al. (2025). Its proportion was higher in oils obtained using the ethanol-based extraction protocol (PU-ET and PE-ET). Considering that the two extraction protocols differed in both solvent and operating conditions, this pattern was interpreted as protocol-dependent and may have been associated with the co-extraction of lipid fractions more strongly linked to structural components (e.g., waxes and complex lipids), which are abundant in outer plant tissues (Molska et al., 2022). Although excessive intake of palmitic acid has been associated with atherogenic effects, it has also been reported as a relevant structural lipid in biological membranes and as a precursor of other lipid-derived compounds, with technological applications in food systems (Cruz et al., 2020; Dimou et al., 2019; Mwaurah et al., 2020; Sousa et al., 2025).

Oleic acid (51.80–63.98%) was the main MUFA in all peach palm oil samples, with the highest proportion observed in PU-ISO. These values were higher than those reported by Sousa et al. (2025) for peach palm pulp oil (54.23%) and by Gualberto et al. (2025) for oil obtained from the seed of the same species (11.08%). Overall, the isooctane-based protocol, particularly for pulp (PU-ISO), yielded a lipid profile with a greater predominance of oleic acid, supporting its nutritional and functional potential among tropical vegetable oils. This trend was consistent with the preferential solubilization of less polar, highly unsaturated lipid species under the isooctane-based protocol, given the affinity of non-polar solvents for long aliphatic chains (El Kourchi et al., 2024). Oleic acid was widely recognized for its health-promoting attributes, including improved lipid markers and anti-inflammatory effects (FAO, 2022; Gualberto et al., 2025; Taboada et al., 2022).

The PUFA fraction was mainly composed of linoleic (ω-6) and α-linolenic (ω-3) acids, both essential fatty acids that must be obtained from the diet. Linoleic acid was found at higher levels in the isooctane-based oils, especially PE-ISO (7.79%) and PU-ISO (7.64%), which again suggested a protocol-dependent selectivity toward less polar lipid species, as discussed by El Kourchi et al. (2024). These results confirmed peach palm oils as relevant sources of essential fatty acids and provided a compositional basis for interpreting their thermal and structural behavior. However, an excessive ω-6/ω-3 intake ratio has been associated with adverse health outcomes, including oxidative stress (Edin et al., 2020). When comparing fractions, peel oils obtained via the ethanol-based protocol (PE-ET) showed the highest SFA proportion, particularly palmitic acid. However, this behavior was not uniform across protocols: PE-ISO had lower SFA levels than PU-ET, whereas PU-ISO had higher MUFA levels, mainly oleic acid. Such protocol- and fraction-dependent profiles could be relevant for targeted applications in food or cosmetic formulations, depending on desired compositional attributes.

Among the evaluated samples, PU-ISO oil showed the highest Nutritional Value Index (NVI), reflecting its comparatively higher proportion of unsaturated fatty acids, especially oleic acid. These fatty acids are associated with reduced LDL cholesterol and inflammation, and they contribute to cardiovascular protection (Chen & Liu, 2020; El Kourchi et al., 2024). In contrast, ethanol-based oils (PU-ET and PE-ET) had lower NVI and H/H values, suggesting a higher proportion of saturated fatty acids and, consequently, a lower potential benefit to the lipid profile. Nevertheless, all oils presented low atherogenic (AI) and thrombogenic (TI) indices (≤1), which indicates a reduced risk of arterial plaque formation and blood clots, due to the relevant presence of mono- and polyunsaturated fats, recognized for their protective action on the cardiovascular system (Amakhmakh et al., 2025; Dal Bosco et al., 2022; Plaha et al., 2023).

Data reported in Table 1 were used to estimate the triacylglycerol (TAG) composition of peach palm pulp and peel oils obtained under the different extraction protocols. It should be emphasized that TAG profiles were predicted using PrOleos software based on fatty acid composition and a random distribution model, rather than experimentally determined by chromatographic analysis. Therefore, these results are ngpresented as estimated TAG profiles and used as supportive evidence for interpreting the thermal and structural behavior of the oils. For TAG

calculation, only fatty acids representing >0.5% of the total peak area were considered (Table 2). A strong agreement was observed between the gas chromatography-based inputs and the TAG predictions generated by the PrOleos software ($r > 0.97$) (Filho et al., 1995). PrOleos includes TAG profiles for a wide range of vegetable oils and their mixtures, particularly those rich in unsaturated fatty acids.

The estimated TAG composition suggested a predominance of mixed saturated–unsaturated triacylglycerols, represented mainly by POO (22.54–29.72%), a monosaturated–diunsaturated TAG, followed by triunsaturated OOO (15.14–26.70%) and disaturated–monounsaturated POP (6.34–19.05%). These results corroborate those obtained by Morais et al. (2024), who investigated oils extracted from different fractions of buritirana (*Mauritiella armata*), and by Sousa et al. (2025), who analyzed the TAG profile of oils from the peel of buriti (*Mauritia flexuosa*), both belonging to the *Arecaceae* family. The similarity observed between the results confirms the data presented in Table 1, since the fatty acid composition showed oleic, linoleic, and palmitic acids as the main constituents.

On the other hand, **the PrOleos-based stereospecific prediction** suggested that oleic and linoleic acids were preferentially located at the *sn*-2 position of the glycerol backbone, a distribution pattern often associated with TAGs of higher nutritional value. This molecular configuration favors intestinal absorption and reduces plasma cholesterol levels, as demonstrated by Chen and Liu (2020) and Polmann et al. (2024). Additionally, the predominance of POO and OOO species confers intermediate plasticity to peach palm oil, typical of semi-solid lipid matrices. This estimated TAG profile may contribute to physicochemical properties desirable for applications in food products requiring a creamy texture, good oxidative stability, and adequate rheological behavior during processing and storage. Thus, the observed triacylglyceride composition reinforces the technological and nutritional potential of peach palm oil as a high-value functional ingredient.

It is important to note that the TAG profiles reported in this study were estimated from fatty acid composition using a random distribution model and were not experimentally determined by chromatographic techniques. Therefore, the predicted TAG composition was used as supportive information to interpret the thermal, crystalline, and rheological behavior of the oils. Direct experimental determination of TAG species, for example, by high-performance liquid chromatography or mass spectrometry-based approaches, would further strengthen the structure–function correlations proposed here.

Table 2
Estimated triacylglycerol composition and β-carotene and lycopene contents of peach palm pulp and peel oils.

Triacylglycerol (*wt%*)	PU-ISO	PU-ET	PE-ISO	PE-ET
PPP	0.59^{d}	4.06^{a}	2.99^{c}	3.76^{b}
PPoP	0.56^{c}	1.80^{a}	1.30^{b}	1.34^{b}
SPP	–	0.54^{a}	–	0.55^{a}
POP	6.34^{d}	19.05^{a}	15.73^{c}	17.97^{b}
PLP	0.75^{c}	2.16^{b}	2.30^{a}	2.23^{ab}
POPo	1.01^{b}	–	4.55^{a}	–
PPoP	–	5.61	–	–
PPoO	–	–	–	4.26
PoOPo	0.63	–	–	–
PLPo	–	0.63^{a}	0.66^{a}	0.52^{b}
PLLP	–	–	0.59^{b}	0.72^{a}
HOP	0.78	–	–	–
SOP	0.79^{c}	1.69^{a}	1.35^{b}	1.75^{a}
POO	22.54^{d}	29.72^{a}	27.52^{c}	28.57^{b}
PLO	5.30^{d}	6.74^{c}	8.06^{a}	7.10^{b}
PoOO	7.13^{a}	–	3.99^{b}	–
OPoO	–	4.39^{a}	–	3.39^{b}
OLPo	–	0.99^{a}	–	0.84^{b}
PLLO	2.50^{a}	–	2.06^{c}	2.30^{b}
PoLO	1.68^{a}	–	1.16^{b}	–
PLL	–	–	0.60	–
PoLLO	0.80	–	–	–
HOO	1.40	–	–	–
SOO	1.41^{a}	1.32^{b}	1.17^{c}	1.39^{a}
OOO	26.70^{a}	15.45^{c}	16.10^{b}	15.14^{c}
OLO	9.42^{a}	5.26^{c}	7,06^{b}	5.64^{c}
OOLn	4.45^{a}	–	1.81^{b}	1.82^{b}
OLL	1.10^{a}	0.60^{d}	1.03^{b}	0.70^{c}
OLLn	1.04	–	–	–
Carotenoids (μg/mL oil)				
β-Carotene	8.55 ± 0.01^{d}	10.77 ± 0.01^{a}	10.53 ± 0.02^{b}	9.87 ± 0.01^{c}
Lycopene	2.76 ± 0.00^{b}	ND	3.37 ± 0.05^{a}	1.99 ± 0.03^{c}

Triacylglycerols composition was estimated using PrOleos software based on the fatty acid composition and a random distribution model; therefore, TAG values should be interpreted as predicted relative profiles rather than experimentally measured TAG concentrations. Data are expressed as mean ± standard deviation ($n = 2$). Equal letters on the same line show no significant difference (Tukey's test and *t*-test, $p < 0.05$). **M**, myristic acid; **P**, palmitic acid; **Po**, palmitoleic acid; **S**, stearic acid; **O**, oleic acid; **L**, linoleic acid; **G**, *cis*-11-eicosenoic acid (gondoic acid); **La**, lauric acid; **Pe**, pentadecanoic acid; **H**, heptadecanoic acid; **A**, arachidonic acid; **Ln**, alpha linolenic acid; **Ga**, gadoleic acid. **Carotenoids** are expressed as mean ± standard deviation ($n = 2$). Different superscript letters within the same line indicate significant differences (**Welch's one-way ANOVA**, $p < 0.05$). **ND**: not detected.

Table 2 reports the concentrations of β-carotene and lycopene in peach palm pulp and peel oils. β-Carotene was the predominant carotenoid in all samples, whereas lycopene occurred at lower levels and was not detected in PU-ET oil (Table 2). β-Carotene content differed among samples ($p < 0.05$), with higher values observed for PU-ET and PE-ISO, intermediate levels for PE-ET, and the lowest concentration for PU-ISO. Lycopene also differed among the oils in which it was detected ($p < 0.05$), reaching the highest level in PE-ISO, followed by PU-ISO and PE-ET, while PU-ET remained not detected (Table 2). Because the extraction procedures differed in solvent polarity, operating conditions, and laboratory context, these differences were interpreted as **protocol-dependent** rather than strictly solvent-driven. Similar matrix- and protocol-related selectivity in carotenoid recovery has been reported for vegetable oils and lipid-rich systems (Freitas et al., 2024; Menezes Silva et al., 2023; Wijngaard et al., 2012).

Differences between pulp and peel oils were consistent with the natural distribution of carotenoids across fruit tissues. Peel tissues, which are more exposed to light and environmental stress, have been reported to accumulate higher levels of photoprotective pigments, which could contribute to the higher lycopene levels observed in peel oils (Miranda et al., 2024; Noronha Matos et al., 2019). The absence of lycopene in PU-ET further suggested that carotenoid recovery depended on the interplay between matrix characteristics and extraction conditions, potentially influencing pigment release and/or degradation during processing. Carotenoids may also have contributed to the physicochemical behavior of these oils, as lipophilic pigments can partition into the liquid phase and, depending on concentration and molecular interactions, affect crystallization and microstructure development. In this sense, previous studies have reported that TAG composition and crystalline organization can modulate the incorporation and stability of lipophilic bioactives in oils and fat-based matrices (Bu et al., 2022; Saini et al., 2022). Overall, peach palm oils showed measurable levels of β-carotene and lycopene, with statistically significant but moderate differences among samples (Table 2).

3.2. Physical properties

Differential scanning calorimetry (DSC) analysis (Fig. 2 and Table 3) revealed complex crystallization and melting behaviors in peach palm peel and pulp oils that depended on the **extraction protocol** and anatomical fraction. The multiple thermal events observed were consistent with the heterogeneous lipid composition of the samples, including the estimated TAG profiles (Table 2), and suggested the coexistence of different crystalline arrangements, as commonly

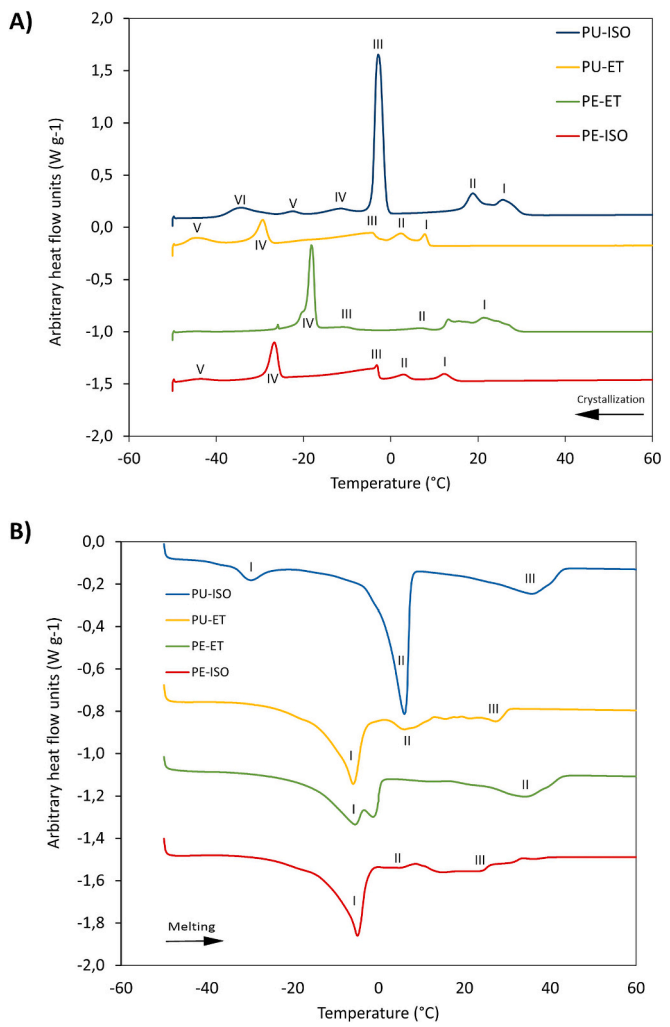

Fig. 2. Crystallization - EXO (A) and melting - ENDO (B) curves by Differential scanning calorimetry (DSC) of peach palm pulp and peel oils.

observed in lipid systems containing a wide distribution of saturated and unsaturated acyl chains (Alarcon et al., 2020; Rajagukguk et al., 2023). From a technological perspective, particular attention was given to the thermal transitions occurring at or above room temperature (≈20 °C), as these events determined whether the oils behaved as liquid or solid/semi-solid fats under practical application conditions (Alarcon et al., 2020; Rajagukguk et al., 2023).

During the crystallization step (Fig. 2A), all oils exhibited exothermic events at subzero temperatures (approximately from −45 to −2 °C), which were consistent with the crystallization of low-melting TAG fractions enriched in unsaturated fatty acids. These low-temperature events **may be associated** with the formation of metastable polymorphic forms (e.g., α and β') in lipid matrices rich in oleic and linoleic acids, and were mainly relevant for frozen food applications, with limited technological relevance at ambient temperature (Bu et al., 2022; Saini et al., 2022). In addition to these subzero events, PU-ISO and PE-ET also showed crystallization peaks in the 20–30 °C range. Specifically, PU-ISO displayed a prominent exothermic event within this interval, and PE-ET showed a crystallization peak around ~21 °C with substantial enthalpy (ΔH up to +19.46 J g^{-1}) (Table 3). These higher-temperature events suggested the crystallization of higher-melting lipid fractions that were expected to contribute more directly to structure formation at ambient conditions. Notably, the magnitude of crystallization enthalpy reflected the extent of crystallization under the applied conditions, whereas polymorphic stability and crystal packing required confirmation by complementary structural analyses.

Table 3
Thermal parameters of oil samples by DSC of peach palm pulp and peel oils.

			PU-ISO	PU-ET	PE-ISO	PE-ET
Crystallization	**Peak 1**	Peak (°C)	27.25	7.87	12.36	21.38
		ΔH (J g^{-1})	+19.48	+1.43	+2.43	+17.23
	Peak 2	Peak (°C)	18.9	2.37	3.02	6.86
		ΔH (J g^{-1})	+22.27	+2.31	+1.65	+0.96
	Peak 3	Peak (°C)	−2.55	−4.3	−3.13	−10.15
		ΔH (J g^{-1})	+39.18	+10.02	+11.19	+0.81
	Peak 4	Peak (°C)	−11.7	−29.29	−26.62	−18.03
		ΔH (J g^{-1})	+2.07	+7.65	+9.78	+19.46
	Peak 5	Peak (°C)	−22.5	−44.9	−43.90	–
		ΔH (J g^{-1})	+0.94	+4.09	+1.45	–
	Peak 6	Peak (°C)	−34.6	–	–	–
		ΔH (J g^{-1})	+6.21	–	–	–
Melting	**Peak 1**	Peak (°C)	−29.86	−5.99	−4.97	−5.55
		ΔH (J g^{-1})	−5.30	−28.71	−28.72	−31.92
	Peak 2	Peak (°C)	5.86	6.13	5.23	34.21
		ΔH (J g^{-1})	−48.15	−3.76	−0.67	−14.11
	Peak 3	Peak (°C)	35.70	27.55	23.23	–
		ΔH (J g^{-1})	−21.29	−3.11	−9.43	–

ΔH values were calculated by peak integration. Positive ΔH indicates exothermic crystallization and negative ΔH indicates endothermic melting. "–" denotes that no peak was detected under the experimental conditions.

The melting profiles (Fig. 2B) clearly distinguished the oils by their room-temperature behavior. **PU-ISO and PE-ET exhibited melting events extending to or above 20 °C, explaining their solid or semi-solid character at room temperature**, whereas PU-ET and PE-ISO showed melting transitions predominantly below 20 °C, confirming a liquid behavior at ambient conditions. The solid character of PU-ISO could be *partially* associated with the formation of a well-connected crystalline network involving organized TAGs, particularly palmitoyl-dioleoyl-glycerol (POO), a monosaturated–diunsaturated TAG, and trioleoyl-glycerol (OOO), a triunsaturated TAG. (Pereira et al., 2019; Polmann et al., 2024). In contrast, the higher melting transitions observed for PE-ET **suggested** a larger contribution of higher-melting TAG fractions (e.g., POP and PPP), which crystallized at higher temperatures and were expected to promote a more structured lipid phase (Rajagukguk et al., 2023; Tomaszewska-Gras et al., 2021). Overall, DSC results indicated that the room-temperature consistency of peach palm oils depended on the combined influence of extraction protocol and fruit fraction, rather than on solvent polarity alone. These thermal trends were subsequently discussed alongside microstructural and scattering/rheological evidence in the following sections.

The apparent discrepancy between the lower SFA content of PU-ISO and its semi-solid behavior at 20 °C indicates that the macroscopic consistency of peach palm oils cannot be explained solely by the global degree of saturation. Instead, the physical state at room temperature is governed by the specific TAG species able to crystallize and remain solid under the applied thermal conditions. In this sense, the estimated TAG profile provides supportive evidence that individual TAG classes, such as

palmitoyl-dioleoyl-glycerol (POO), dipalmitoyl-oleoyl-glycerol (POP), and tripalmitoyl-glycerol (PPP), may contribute differently to crystallization, depending on their melting ranges, molecular packing, and ability to participate in mixed crystal networks. Although PU-ET showed a higher overall SFA content, this parameter alone does not necessarily translate into a higher solid fraction at 20 °C, because the distribution, compatibility, and crystallization kinetics of TAG species also determine the amount and connectivity of crystals formed during cooling. Therefore, the semi-solid behavior of PU-ISO was attributed to the formation of a connected crystal network rather than to SFA content alone.

The concept of solid fat content (SFC) is particularly relevant for rationalizing these differences, since oils with similar global fatty acid saturation may display distinct macroscopic consistencies depending on the fraction of crystalline material retained at a given temperature. In the present study, SFC was not directly measured; therefore, the room-temperature behavior was inferred from DSC transitions, PLM micrographs, SAXS/XRD structural features, and rheological measurements performed for the structured samples. Future studies, including direct SFC determination, for example, by pulsed nuclear magnetic resonance, would provide a more quantitative basis for relating TAG composition, crystallization behavior, and macroscopic consistency in peach palm oils.

PLM micrographs acquired at 20 °C showed marked differences in crystal morphology and density among peach palm pulp and peel oils as a function of the **extraction protocol** (Fig. 3). In general, birefringent domains typical of crystallized TAG structures were observed, with distinct patterns across samples. PU-ISO exhibited elongated, needle-like crystals heterogeneously distributed, with the formation of branched aggregates, suggesting the coexistence of multiple crystalline populations and a well-developed network at 20 °C (Fig. 3B). This microstructure was consistent with the DSC profiles, which showed crystallization/melting events extending to around room temperature for PU-ISO, supporting its structured character under ambient conditions (Fig. 2 and Table 3). The prevalence of fine, elongated crystals has been reported in lipid systems enriched in unsaturated TAGs, where reduced intermolecular packing tends to favor smaller, less symmetric crystal morphologies (Domingues et al., 2022).

On the other hand, the PU-ET micrograph revealed extremely fine, uniformly distributed crystals with intense anisotropic brightness, suggesting a more homogeneous crystal field at 20 °C (Fig. 3A). The lower enthalpy of crystallization ($\Delta H = 2.31$ J g^{-1}) and the shift of the melting peaks to lower temperatures (−5.99 °C) confirm the presence of smaller and more ordered crystals, characteristic of the predominant transition to the β' polymorph, similar to that found in palm oil cooled to 20 °C by De Witte, Penagos, Rondou, et al. (2024). This behavior may be related to the protocol's polar nature, which interferes with intermolecular interactions between TAGs and alters nucleation during crystal formation (Zeb & Murkovic, 2011). The PE-ISO oil presented large, radiating crystals with needle-like morphology and a star-like appearance, indicative of a less compact structure and incomplete crystallization field at 20 °C (Fig. 3D). This morphology is associated with the high concentration of unsaturated fatty acids and TAGs with double bonds, whose insertion between the acyl chains interferes with nucleation and crystal growth (Pinna et al., 2025). The irregular birefringence and dark zones observed suggested the coexistence of amorphous and semi-crystalline regions (Polińska et al., 2021), consistent with the greater thermal disorder detected in the DSC (multiple peaks and ΔH variable between 1.45 and 11.19 J g^{-1}), as observed in the chromoplasts of mango and papaya by Schweiggert et al. (2012).

In contrast, the PE-ET oil exhibited a micrographic field dominated by small, compact, and strongly birefringent crystals with a uniform granular pattern (Fig. 3C), like that observed in sunflower oil by Biswas et al. (2017). This structure evidences a more stable and energetically favorable system, in agreement with the DSC, which showed higher crystallization peaks (10.0–21.0 °C) and considerable enthalpy ($\Delta H = 17.23$ J g^{-1}). Because the extraction procedures differed in solvent and operating conditions (and were performed in different laboratories), these differences were discussed as protocol-dependent rather than strictly solvent-driven (Gomaa et al., 2022; Pinna et al., 2025). Taken together, the PLM micrographs confirm the strong influence of the extraction protocol and the fruit fraction on the morphology and spatial distribution of crystals. The isooctane-based protocol was associated

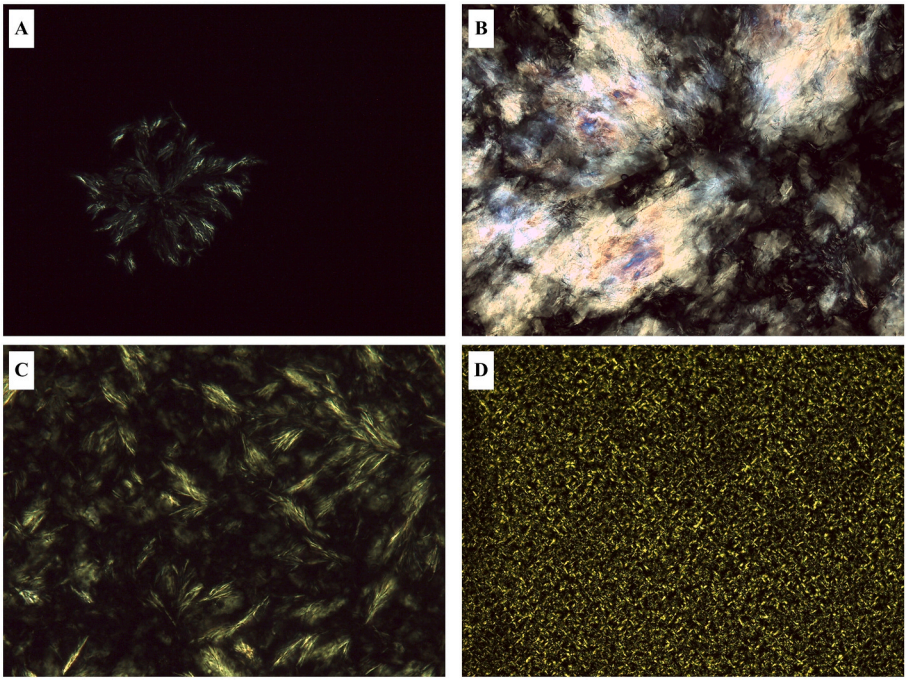

Fig. 3. Polarized light microscopy (PLM) micrographs of peach palm oils obtained from pulp and peel using different extraction protocols: (A) pulp oil obtained by the ethanol-based protocol (PU-ET), (B) pulp oil obtained by the isooctane-based protocol (PU-ISO), (C) peel oil obtained by the ethanol-based protocol (PE-ET), and (D) peel oil obtained by the isooctane-based protocol (PE-ISO). Micrographs were recorded at 20 °C.

with more disordered and heterogeneous structures due to the greater extraction of unsaturated compounds, while the ethanol-based protocol resulted in more organized and compact systems. These findings corroborate the DSC results and demonstrate that fatty acid content modulates lipid crystallization, influencing both thermal stability and optical anisotropy. The observation of distinct birefringence patterns and crystal sizes across the samples also indicates the presence of distinct TAG polymorphs, a phenomenon that can be confirmed and quantified by SAXS and XRD structural analyses.

The structural characterization of the oils extracted from peach palm peel and pulp using solvents of different polarities was conducted using SAXS, and the results were analyzed according to Porod's Law (Fig. 4 and Table 4). The result could be relatively well fitted on a log-log scale to the I(q) curve as a function of q, allowing investigation of the degree of interface definition in lipid systems (Santos et al., 2021). The relationship $I(q) \sim q^{-n}$, in which the exponent $n = 6 - d_s$ is associated with the nature and regularity of the interfaces between domains of contrasting electron density. The exponent gives information about the surface fractal dimension d_s which is 2 for smooth surfaces ($n = 4$) and higher values up to 3 ($n = 3$) for highly rough surfaces. Thus, the exponent reveals differences in the internal organization of the samples depending on the portion of the fruit used and the type of solvent employed in the extraction process (Silva et al., 2024).

The comparison between the structural data obtained by SAXS and PLM images (Fig. 3 and Fig. 4) reveals important information about the supramolecular organization and morphology of the oils extracted from peach palm pulp and peel by using different solvents. The analysis using the Guinier equation complements the structural characterization of the samples by providing an estimate of the radius of gyration (Rg) (Table 4), representative of the average size of the domains or aggregates present in the oils (Heiden-Hecht et al., 2024; Mastrangelo et al., 2020). The values obtained showed good agreement with the structural observations from the SAXS data and PLM images. The PU-ISO presented the steepest Porod slope ($n = -3.78$; $R^2 = 0.999$) and a radius of gyration (Rg) of 117 nm, indicating well-defined interfaces. This result suggests that the isooctane-based protocol was associated with more defined interfacial organization, possibly reflecting differences in the lipid fractions recovered under this protocol (Andrade & Negrão, 2025; Liu et al., 2023). The PLM image (Fig. 3B) corroborates this finding, exhibiting small, dense, and strongly birefringent crystals. This compact organization is associated with the predominance of POO and OOO-type TAGs, as well as the high oleic acid content (63.98%), which promotes molecular flexibility without compromising acyl chain packing (Andrade & Negrão, 2025; Liu et al., 2023).

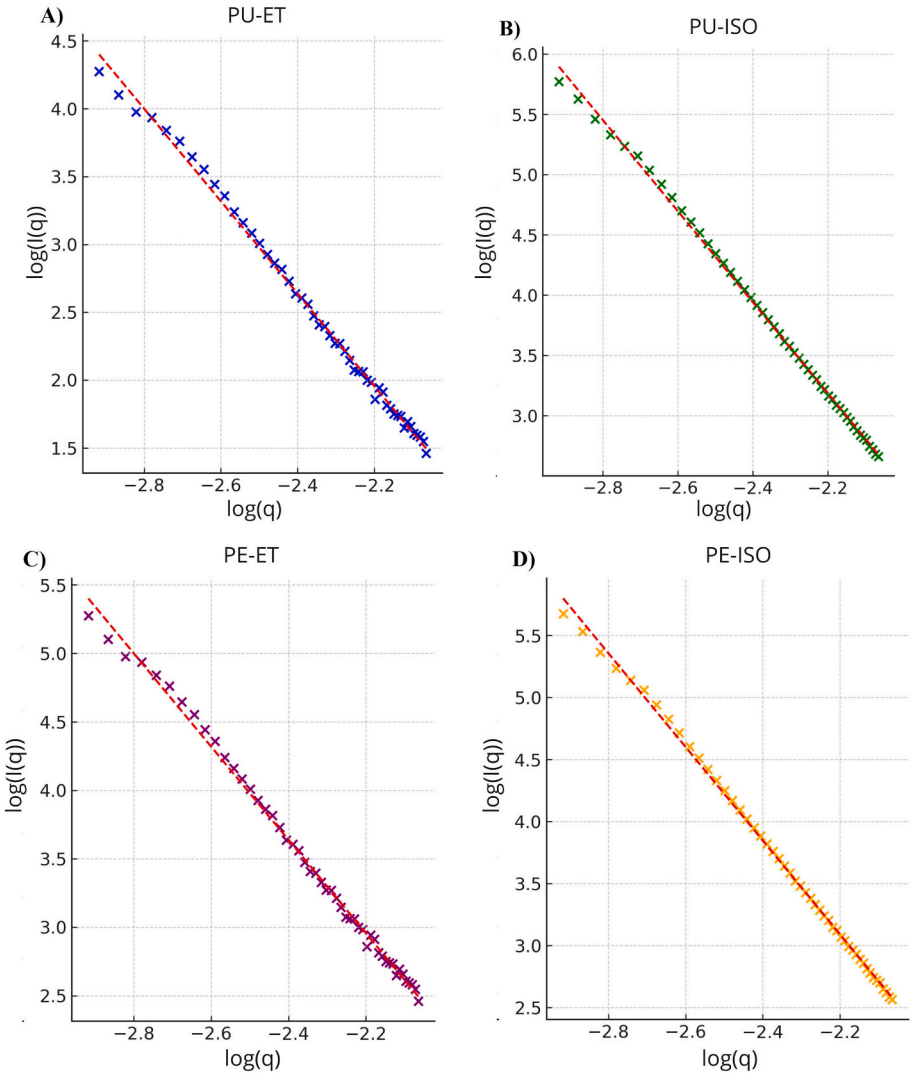

Fig. 4. Power-law regime plots of peach palm oils obtained from pulp and peel using different extraction protocols: (A) pulp oil obtained by the ethanol-based protocol (PU-ET), (B) pulp oil obtained by the isooctane-based protocol (PU-ISO), (C) peel oil obtained by the ethanol-based protocol (PE-ET), and (D) peel oil obtained by the isooctane-based protocol (PE-ISO). Measurements were performed at 20 °C.

Table 4
Synthesis of the correlation between SAXS (Porod and Guinier regimes), PLM, and XRD from pulp and peel oils of peach palm.

–	SAXS				XRD	
Samples	Porod exponent (*n*)	Rg (nm)	PLM	Interpretation	Q ($Å^{-1}$)	d (Å)
PU-ET	−3.41	107	Long and oriented domains	Partially ordered structure	0.15 0.22 0.42 1.35	41.9 28.6 15.0 4.65
PU-ISO	−3.78	117	Small, dense crystals	High organization and regular interfaces	0.15 0.22 0.42 1.35	41.9 28.6 15.0 4.65
PE-ET	−3.15	123	Heterogeneous, birefringent	Diffuse interfaces, irregular structure	0.15 0.22 0.42 1.38	41.9 28.6 15.0 4.55
PE-ISO	−3.47	115	Clustered crystals	Moderate order with crowding	0.15 0.22 0.42 1.38	41.9 28.6 15.0 4.55

PU-ET showed a lower Porod slope ($n = -3.41$; $R^2 = 0.997$) and an Rg of 107 nm, indicating fewer regular interfaces and elongated domains. This difference may be associated with the greater presence of polar compounds and the lower fraction of unsaturated TAGs, which introduce heterogeneity into the lamellar arrangement. Ethanol, by interacting with polar lipids and protein or phospholipid residues, tends to generate less cohesive microdomains, as reflected in PLM images showing thin, oriented crystals with lower optical density. In the peel samples, a reverse trend was observed. The PE-ISO showed $n = -3.47$ ($R^2 = 0.999$) and Rg of 115 nm, indicating a moderately ordered structure with agglomerated crystals and well-defined interfaces, although less uniform than those of the pulp. This behavior may reflect the balance between the lipid network and the estimated proportion of mixed saturated–unsaturated and unsaturated TAGs (POO, OOO, POP), which favor molecular plasticity (Bu et al., 2022; Saini et al., 2022). On the other hand, the PE-ET presented the lowest degree of interface definition ($n = -3.15$; $R^2 = 0.98$) and the highest Rg (123 nm), suggesting diffuse and heterogeneous structures. This morphology, also observed in the PLM through irregular birefringent domains, can be attributed to the greater diversity of compounds extracted with the polar solvent, such as phospholipids, oxidized pigments, and short-chain lipids, which promote partial disruption of the lamellar organization (Andrade & Negrão, 2025; Freitas et al., 2024).

The results from SAXS in low and high are consistent with the thermal and morphological data previously discussed: oils with higher unsaturation content (PU-ISO and PE-ISO) present less dense packing and well-defined interfaces, while those with higher saturation and extracted with ethanol (PU-ET and PE-ET) exhibit more compact but less uniform structures (De Witte, Penagos, Rondou, et al., 2024; Olsmats et al., 2025). This structural modulation is a direct result of solvent selectivity, which controls the relative proportion of unsaturated (SU_2 and U_3) and saturated (S_2U and S_3) TAGs and, consequently, the degree of ordering of the lipid matrix. On the other hand, more disorganized structures can facilitate the incorporation of polar bioactive compounds or facilitate dispersion in hydrophilic matrices, albeit with lower physicochemical stability (Olsmats & Rennie, 2024; Rondou et al., 2024). Thus, the extraction protocol influenced not only the yield and chemical composition of the oil but also its nanostructure, directly impacting its technological and functional properties.

XRD scattering analysis was performed to investigate the presence of ordered phases in the oils extracted from the pulp and peel of peach palm, considering the influence of the extraction solvents ethanol and isooctane. In all diffractograms (Fig. 5), distinct shoulders were observed in the region of Q ≈ 0.15, 0.22, 0.42, and 1.35–1.38 $Å^{-1}$,

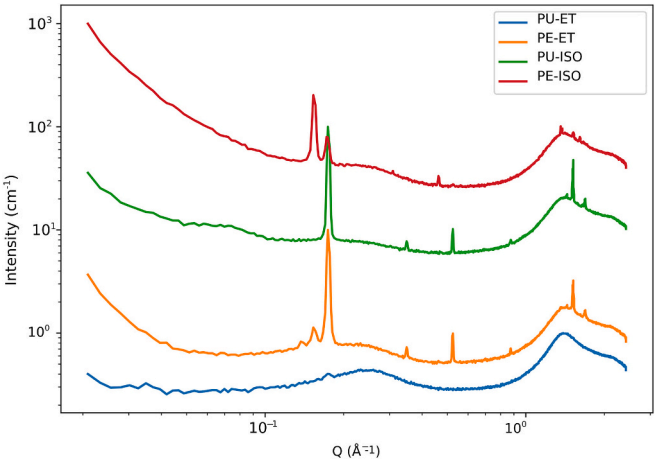

Fig. 5. Wide-angle X-ray scattering (XRD) graph from pulp and peel oils of peach palm.

which correspond to crystalline or semicrystalline structures present in the oils (Ferreira & da Silva, 2023). Table 4 presents the estimated values of interplanar spacing (d), calculated based on the Bragg equation ($d = 2\pi/Qd = 2\pi/Qd = 2\pi/Q$). The spacings obtained were approximately 41.9, 28.6, 15.0, and 4.6 Å (Table 4), indicating the coexistence of long-range lamellar structures and more compact molecular packings for all samples.

The peak located at Q ≈ 1.35–1.38 $Å^{-1}$ (d ≈ 4.6 Å) is commonly associated with the packing of the acyl chains of triacylglycerols (TAGs) (De Witte, Penagos, Rondou, et al., 2024; De Witte, Penagos, Van de Walle, et al., 2024), and suggests the presence of β or β' type crystalline phases, which are typical in partially crystallized lipids (Domingues et al., 2022; Peyronel et al., 2023). The lower Q peaks, in turn, may be related to the lamellar organization of lipids, vesicles, or structured aggregates, evidencing the existence of regions of supramolecular ordering in the analyzed oils (De Witte, Penagos, Rondou, et al., 2024; De Witte, Penagos, Van de Walle, et al., 2024; Mazzanti, 2021). The presence and position of the peaks were similar between the oils extracted with ethanol and isooctane, for both the pulp and the peel. However, differences in peak relative intensities suggest that the type of solvent can affect the proportions of crystalline phases or the extent of organization without destroying the structure (Zhang et al., 2025). Specifically, the oils extracted with isooctane (PE-ISO and PU-ISO)

showed more defined peaks in some regions, suggesting greater preservation of the ordered lipid phases, as this nonpolar solvent tends to preserve the integrity of native structures.

Overall, XRD analyses revealed that the isooctane-based protocol tended to a more regular nanostructure and well-defined interfaces, whereas ethanol-based oils resulted in greater heterogeneity and lower crystallinity. This structural modulation may affect the technological properties of the oils, indicating that more ordered systems would exhibit greater thermal and oxidative stability, whereas more disordered systems would favor the incorporation of bioactive compounds and their dispersion in hydrophilic matrices. Thus, the supramolecular structure of peach palm oils is likely to reflect the synergistic interactions among the chemical composition (fatty acids and TAGs), bioactive pigments, and the extraction solvent, demonstrating the potential of these oils as multifunctional ingredients for food and cosmetic applications.

To probe the technological potential of the extracted oils, oscillatory rheological analysis was conducted at 20 °C **only for the samples that exhibited a structured (solid/semi-solid) character at this temperature**, namely peach palm pulp (PU-ISO) and peel (PE-ET) oils (Fig. 6). As shown in Fig. 6, both samples presented elastic modulus (G′) values higher than viscous modulus (G″) across the entire frequency range (0.1–100 Hz), indicating predominantly elastic behavior. Such behavior can be attributed to a cohesive microstructure able to withstand moderate oscillatory deformation without irreversible structural breakdown (Pommella et al., 2020).

The PU-ISO sample presented high G′ values, reaching almost 80,000 Pa at 1 Hz, whereas G″ remained low and practically constant throughout the entire analyzed frequency range (Fig. 6). These values **fell within** the range of other tropical oils conventionally used as plastic fats in food formulations (Attia et al., 2020). The reported behavior suggests the formation of a strongly structured and mechanically resistant lipid network, consistent with the SAXS results, and may be associated with the presence of small, densely packed crystals observed by polarized light microscopy and with the *estimated* high proportion of organized TAG species, POO a monosaturated–diunsaturated TAG, and OOO, a triunsaturated TAG. These TAGs may contribute to molecular packing arrangements compatible with the structured behavior observed at 20 °C (De Witte, Penagos, Van de Walle, et al., 2024). The high concentration of oleic acid (63.98%) and β' may also contribute to network rigidity, as these compounds modulate intermolecular interactions and stabilize organized lipid domains (Andrade & Negrão, 2025; Guimarães et al., 2023).

On the other hand, PE-ET oil exhibited lower G′ values (~ 3700 Pa) at 1 Hz, accompanied by an increase in G″ at higher frequencies, indicating a weaker structure and more fluid behavior. This profile is characteristic of systems with greater energy dissipation and lower crystalline connectivity, possibly resulting from disruption of lipid self-assembly by polar compounds extracted using an ethanol-based protocol (Andrade & Negrão, 2025; Li et al., 2022; Liu et al., 2023). This interpretation was consistent with SAXS and XRD analyses, which revealed more diffuse interfaces, a larger radius of gyration, and less intense Bragg peaks, indicating a lower degree of crystallinity and greater structural heterogeneity.

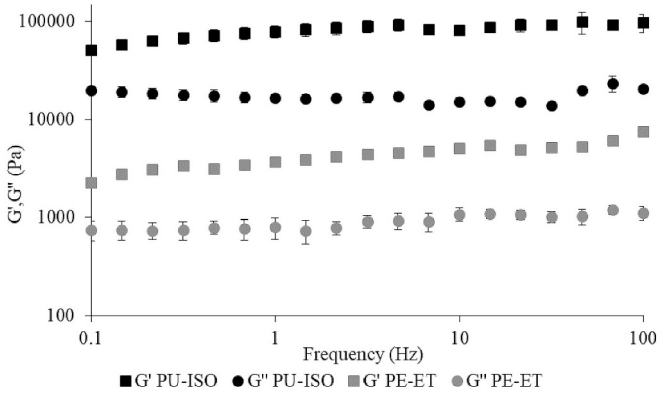

Fig. 6. Evolution of the storage modulus G' (square points) and the loss modulus G" (round points) as a function of oscillation frequency for samples of peach palm oils at 20 °C.

It is important to acknowledge that the two extraction procedures compared in this study differed not only in solvent polarity but also in operating conditions, including extraction time, temperature, and mechanical energy input. Therefore, the observed differences in yield, chemical composition, carotenoid recovery, thermal behavior, and structural organization should be interpreted as the result of the overall extraction protocol rather than as the isolated effect of solvent polarity. Accordingly, throughout the manuscript, comparisons were framed as isooctane-based versus ethanol-based protocols. Future studies using controlled experimental designs in which solvent type, temperature, extraction time, and mechanical treatment are varied independently would be necessary to isolate the contribution of each factor to the composition and structure–function behavior of peach palm oils.

4. Conclusions

The results of this study showed that the composition, supramolecular organization, and technological functionality of peach palm oils depended on the fruit fraction and the **extraction protocol**. The oils exhibited high oleic acid content, which was associated with favorable nutritional lipid indices, including low atherogenicity and thrombogenicity, and comparatively high H/H ratios. In addition, measurable levels of carotenoids (β-carotene and lycopene) highlighted the potential of these oils as sources of lipophilic bioactive compounds. Across samples, differences in predicted TAG distribution and fatty-acid profiles were reflected in thermal transitions (DSC), crystal morphology (PLM), and nanostructural/crystalline features (SAXS/XRD), supporting a consistent relationship between degree of unsaturation, ordering of lipid assemblies, and **physical/structural stability at room temperature**. Rheological analysis was conducted only for the samples that exhibited structured behavior at 20 °C, namely PU-ISO and PE-ET. PU-ISO exhibited a more structured behavior at 20 °C, as indicated by melting/crystallization events extending toward room temperature and by the development of an interconnected crystalline network. In contrast, PE-ET showed a weaker viscoelastic network and more heterogeneous structural signatures, despite exhibiting thermal events near room temperature, highlighting the combined role of matrix fraction and extraction conditions in determining oil organization. Overall, this work provides an integrative characterization of peach palm pulp and peel oils by correlating chemical composition with multiscale structural and rheological behavior. The findings reinforce the peel as a valuable lipid source with relevance to future circular bioeconomy strategies, supporting its use in functional foods and cosmetic formulations within this framework.

CRediT authorship contribution statement

Hermanny Matos Silva Sousa: Writing – original draft, Visualization, Validation, Investigation, Formal analysis, Data curation, Conceptualization. **Rômulo Alves Morais:** Writing – review & editing, Writing – original draft, Validation, Formal analysis, Data curation. **Federico Basso:** Visualization, Validation, Investigation, Formal analysis, Data curation, Conceptualization. **Roberta Pratolino:** Visualization, Validation, Investigation, Formal analysis, Data curation. **Luana Regina Pereira Alves:** Visualization, Validation, Investigation, Formal analysis, Data curation. **Gabriela Fonsêca Leal:** Visualization, Validation, Investigation, Formal analysis, Data curation. **Monica Anese:** Writing – review & editing, Visualization, Supervision. **Fabiana Queiroz:** Writing – review & editing, Visualization, Supervision, Project administration. **Paulo Peres de Sá Peixoto:** Writing – review & editing,

Visualization, Supervision, Project administration. **Sonia Calligaris:** Writing – review & editing, Visualization, Supervision, Project administration. **Glêndara Aparecida de Souza Martins:** Writing – review & editing, Visualization, Supervision, Resources, Project administration, Conceptualization.

Declaration of competing interest

The authors declare that they have no known competing financial interests or personal relationships that could have appeared to influence the work reported in this paper.

Acknowledgments

Sousa, H.M.S., thanks the National Council for Scientific and Technological Development (CNPq/Brazil) for the doctoral scholarship (Process number: 140267/2022-0) and acknowledges the Federal University of Lavras (UFLA, Brazil), the Federal University of Tocantins (UFT, Brazil), and the University of Udine (Italy) for institutional and research support. Leal, G.F., received funding from CAPES/Brazil for the doctoral scholarship (grant no. 88887.959518/2024-00). Martins, G.A. S., received funding and thanks to the National Council for Scientific and Technological Development - CNPq, Call CNPq/MCTI/FNDCT No. 22/2024 - Knowledge Brazil Program, process: (443124/2024-8). TheTocantins Research Foundation (FAPT) through the Rosas na Ciência Call (Notice No. 001/2024; CNPJ/MF: 13.664.245/0001-65), and by FINEP through the calls Program for Recovery and Expansion of Scientific and Technological Research Infrastructure in Universities and ICTs (PRÓ-INFRA) and MCTI/FINEP/FNDCT/Transversal Action – Infrastructure for the Legal Amazon 2024 (PRÓ-AMAZON). Queiroz, F., thanks the Minas Gerais State Research Support Foundation (FAPEMIG/Brazil) for funding the project (Process number - APQ 00149-22). Peixoto, P.P.S., acknowledges financial support from GDR2019 CNRS/INRAE "Solliciter LA Matière Molle" (SLAMM) and from the Synchrotron Soleil (beamline SWING). The Authors would like to also thank Dr. Erica Moret from the University of Udine for the analytical support in the determination of fatty acids.

Data availability

Data will be made available on request.

References

Alarcon, R. T., Gaglieri, C., Lamb, K. J., North, M., & Bannach, G. (2020). Spectroscopic characterization and thermal behavior of baru nut and macaw palm vegetable oils and their epoxidized derivatives. *Industrial Crops and Products, 154*, Article 112585. https://doi.org/10.1016/j.indcrop.2020.112585

Amakhmakh, M., El Kourchi, C., Hajib, A., Harhar, H., El Asri, M., Singh, J., … Meliani, A. (2025). Comparative analysis of lipid profile and nutritional quality of eight Moroccan varieties of *Punica granatum*. *Journal of Food Composition and Analysis, 138*, Article 107008. https://doi.org/10.1016/j.jfca.2024.107008

Andrade, D. E. V., & Negrão, C. O. R. (2025). Rheology of waxy oils: A critical review. *Applications in Engineering Science, 21*, Article 100202. https://doi.org/10.1016/j.apples.2024.100202

Attia, N. K., El-Mekkawi, S. A., Elardy, O. A., & Abdelkader, E. A. (2020). Chemical and rheological assessment of produced biolubricants from different vegetable oils. *Fuel, 271*, Article 117578. https://doi.org/10.1016/j.fuel.2020.117578

Biswas, N., Cheow, Y. L., Tan, C. P., Kanagaratnam, S., & Siow, L. F. (2017). Cocoa butter substitute (CBS) produced from palm mid-fraction/palm kernel oil/palm stearin for confectionery fillings. *Journal of the American Oil Chemists' Society, 94*(2), 235–245. https://doi.org/10.1007/s11746-016-2940-4

Bot, F., Verkerk, R., Mastwijk, H., Anese, M., Fogliano, V., & Capuano, E. (2018). The effect of pulsed electric fields on carotenoids bioaccessibility: The role of tomato matrix. *Food Chemistry, 240*, 415–421. https://doi.org/10.1016/j.foodchem.2017.07.102

Bu, X., Lin, J., Duan, C., Koffas, M. A. G., & Yan, G. (2022). Dual regulation of lipid droplet-triacylglycerol metabolism and ERG9 expression for improved β-carotene production in Saccharomyces cerevisiae. *Microbial Cell Factories, 21*(1), 3. https://doi.org/10.1186/s12934-021-01723-y

Chen, J., & Liu, H. (2020). Nutritional indices for assessing fatty acids: A Mini-review. *International Journal of Molecular Sciences, 21*(16), 5695. https://doi.org/10.3390/ijms21165695

Cruz, M. B., da Oliveira, W. S., Araújo, R. L., Honório França, A. C., & Pertuzatti, P. B. (2020). Buriti (*Mauritia Flexuosa* L.) pulp oil as an immunomodulator against enteropathogenic Escherichia coli. *Industrial Crops and Products, 149*, Article 112330. https://doi.org/10.1016/j.indcrop.2020.112330

Dal Bosco, A., Cartoni Mancinelli, A., Vaudo, G., Cavallo, M., Castellini, C., & Mattioli, S. (2022). Indexing of fatty acids in poultry meat for its characterization in healthy human nutrition: A comprehensive application of the scientific literature and new proposals. *Nutrients, 14*(15), 3110. https://doi.org/10.3390/nu14153110

De Witte, F., Penagos, I. A., Rondou, K., Moens, K., Lewille, B., Tzompa-Sosa, D. A., … Dewettinck, K. (2024). Insights in the structural hierarchy of statically crystallized palm oil. *Crystals, 14*(2), 142. https://doi.org/10.3390/cryst14020142

De Witte, F., Penagos, I. A., Van de Walle, D., Skirtach, A. G., Dewettinck, K., & Van Bockstaele, F. (2024). From Nucleation to Fat Crystal Network: Effects of Stearic–Palmitic Sucrose Ester on Static Crystallization of Palm Oil. *Foods, 13*(9), Article 1372. https://doi.org/10.3390/foods13091372

Dimou, C., Karantonis, H. C., Skalkos, D., & Koutelidakis, A. E. (2019). Valorization of fruits by-products to unconventional sources of additives, oil, biomolecules and innovative functional foods. *Current Pharmaceutical Biotechnology, 20*(10), 776–786. https://doi.org/10.2174/1389201020666190405181537

Domingues, M. A. F., da Silva, T. L. T., Chiu, M. C., Ribeiro, A. P. B., & Gonçalves, L. A. G. (2022). Tailoring crystallization and physical properties of palm mid-fraction with sorbitan tristearate and sucrose stearate. *Food Chemistry, 369*, Article 130943. https://doi.org/10.1016/j.foodchem.2021.130943

Edin, M. L., Duval, C., Zhang, G., & Zeldin, D. C. (2020). Role of linoleic acid-derived oxylipins in cancer. *Cancer and Metastasis Reviews, 39*(3), 581–582. https://doi.org/10.1007/s10555-020-09904-8

El Kourchi, C., Belhoussaïne, O., Elhrech, H., Harhar, H., Ullah, R., Bari, A., Maggi, F., Caprioli, G., Bouyahya, A., & Tabyaoui, M. (2024). Antidiabetic, antioxidant, and phytochemical profile of Pennisetum glaucum cultivated in Central-Southern Morocco and imported from India. *Journal of Agriculture and Food Research, 16*, Article 101197. https://doi.org/10.1016/j.jafr.2024.101197

FAO, F. A. A. O. (2022). *Food and agriculture Organization of the United Nations* (Fats and fatty acids in human nutrition).

Ferreira, C. M., & da Silva, G. J. (2023). Absorption of essential oils in Laponite: Stability enhancement and structural characteristics. *Applied Clay Science, 238*, Article 106936. https://doi.org/10.1016/j.clay.2023.106936

Filho, N. R. A., Mendes, O. L., & Lanças, F. M. (1995). Computer prediction of triacylglycerol composition of vegetable oils by HRGC. *Chromatographia, 40*(9–10), 557–562. https://doi.org/10.1007/BF02290268

Freitas, L. C., dos Santos, R. W. S., Reis, F. R., Haminiuk, C. W. I., Corazza, M. L., & Masson, M. L. (2024). Green extraction technologies: A path to the Amazon bioeconomy development. *Trends in Food Science & Technology, 147*, Article 104462. https://doi.org/10.1016/j.tifs.2024.104462

Gomaa, E., Fathi, H. A., Eissa, N. G., & Elsabahy, M. (2022). Methods for preparation of nanostructured lipid carriers. *Methods, 199*, 3–8. https://doi.org/10.1016/j.ymeth.2021.05.003

Gualberto, L. S., Ibiapina, A., Dias, B. B., Freitas, B. C. B., Melo Filho, A. A., Morais, R. A., & Martins, G. A. S. (2025). Investigation of the physicochemical, bioactive properties and antioxidant potential of seeds of native fruits from Brazil: a study on the tucumã (*Astrocaryum vulgare*), bacupari (*Garcinia gardneriana*) and pupunha (*Bactris gasipaes*). *Anais da Academia Brasileira de Ciências, 97*(1). https://doi.org/10.1590/0001-3765202520240862

Guimarães, A. S., Marinho, T. O., Melo, P. A., Thompson, R. L., de Oliveira, M. C. K., & Nele, M. (2023). Prediction of yield stress of waxy gels in pipelines using scaling theory and crystallization kinetics. *Geoenergy Science and Engineering, 226*, Article 211791. https://doi.org/10.1016/j.geoen.2023.211791

Heiden-Hecht, T., Wu, B., Schwärzer, K., Förster, S., Kohlbrecher, J., Holderer, O., & Frielinghaus, H. (2024). New insights into protein stabilized emulsions captured via neutron and X-ray scattering: An approach with β-lactoglobulin at triacylglyceride-oil/water interfaces. *Journal of Colloid and Interface Science, 655*, 319–326. https://doi.org/10.1016/j.jcis.2023.10.155

Ibiapina, A., da Gualberto, L. S., Dias, B. B., Freitas, B. C. B., de Martins, G. A. S., & Melo Filho, A. A. (2021). Essential and fixed oils from Amazonian fruits: Proprieties and applications. *Critical Reviews in Food Science and Nutrition, 0*(0), 1–13. https://doi.org/10.1080/10408398.2021.1935702

Li, H.-Y., Xie, Q.-B., Sun, H., Guo, W., Yan, F., Miao, Q., Nie, C.-F., Zhuang, Y., Huang, Q., & Zhang, J.-J. (2022). A nonlinear creep damage model for gelled waxy crude. *Petroleum Science, 19*(4), 1803–1811. https://doi.org/10.1016/j.petsci.2021.12.027

Liu, H., Li, H., Li, Q., Wang, K., Wang, Z., Yang, F., Wu, X., Xie, Y., & Zhang, J. (2023). A comprehensive assessment for the structural change of waxy crude oils induced by pour point depressant beneficiation. *Geoenergy Science and Engineering, 228*, Article 211999. https://doi.org/10.1016/j.geoen.2023.211999

Mastrangelo, R., Chelazzi, D., Poggi, G., Fratini, E., Pensabene Buemi, L., Petruzzellis, M. L., & Baglioni, P. (2020). Twin-chain polymer hydrogels based on poly(vinyl alcohol) as a new advanced tool for the cleaning of modern and contemporary art. *Proceedings of the National Academy of Sciences, 117*(13), 7011–7020. https://doi.org/10.1073/pnas.1911811117

Mazzanti, G. (2021). Prenucleation structuring in liquid Triacylglycerols: Navigating a non-ideal landscape. *Journal of the American Oil Chemists' Society, 98*(60).

Menezes Silva, J. V., Silva Santos, A., Araujo Pereira, G., & Campos Chisté, R. (2023). Ultrasound-assisted extraction using ethanol efficiently extracted carotenoids from peels of peach palm fruits (*Bactris gasipaes* Kunth) without altering the qualitative

carotenoid profile. *Heliyon, 9*(4), Article e14933. https://doi.org/10.1016/j.heliyon.2023.e14933

Miranda, P., Morais, R., Sousa, H., Gualberto, L., Freitas, B., Asquieri, E., Martins, G., Boas, E., & Damiani, C. (2024). Effects of pectinase treatment on the optimization and extraction of pigments from Bacupari, Tucumã, and peach palm using response surface methodology. *Journal of the Brazilian Chemical Society.*. https://doi.org/10.21577/0103-5053.20230124

Molska, M., Reguła, J., Grygier, A., Muzsik-Kazimierska, A., Rudzińska, M., & Gramza-Michałowska, A. (2022). Effect of the addition of buckwheat sprouts modified with the addition of Saccharomyces cerevisiae var. boulardii to an Atherogenic diet on the metabolism of sterols, Stanols, and fatty acids in rats. *Molecules, 27*(14), 4394. https://doi.org/10.3390/molecules27144394

Montoro-Alonso, S., Expósito-Almellón, X., Martínez-Baena, D., Martínez-Martí, J., Rueda-Robles, A., Pérez-Gálvez, R., Quirantes-Piné, R., & Lozano-Sánchez, J. (2025). Bioactive enrichment and sustainable processing of vegetable oils: New Frontiers in Agri-food technology. *Foods, 14*(5), 769. https://doi.org/10.3390/foods14050769

Morais, R. A., Lopes Teixeira, G., de Souza, A., Martins, G., Ferreira, R. S., & S., & Mara Block, J.. (2024). Comprehensive evaluation of the chemical profile and antioxidant potential of Buritirana (*Mauritiella armata)*, an underexplored fruit from Brazilian Cerrado. *Food Research International, 179*, Article 113945. https://doi.org/10.1016/j.foodres.2024.113945

Morais, R. A., Sousa, H. M. S., Alves, L. R. P., & Martins, G. A. S. (2025). Emerging trends in the valorization of Brazilian native fruits and nuts: Innovative extraction technologies and green solvents for the recovery of lipids and bioactive compounds. *Trends in Food Science & Technology*. , Article 105238. https://doi.org/10.1016/j.tifs.2025.105238

Morais, R. A., Teixeira, G. L., Ferreira, S. R. S., Cifuentes, A., & Block, J. M. (2022). Nutritional composition and bioactive compounds of native Brazilian fruits of the Arecaceae family and its potential applications for health promotion. *Nutrients, 14*(19), 4009. https://doi.org/10.3390/nu14194009

Mwaurah, P. W., Kumar, S., Kumar, N., Panghal, A., Attkan, A. K., Singh, V. K., & Garg, M. K. (2020). Physicochemical characteristics, bioactive compounds, and industrial applications of mango kernel and its products: A review. *Comprehensive Reviews in Food Science and Food Safety, 19*(5), 2421–2446. https://doi.org/10.1111/1541-4337.12598

Noronha Matos, K. A., Praia Lima, D., Pereira Barbosa, A. P., Zerlotti Mercadante, A., & Campos Chisté, R. (2019). Peels of Tucumã (*Astrocaryum vulgare*) and peach palm (*Bactris gasipaes*) are by-products classified as very high carotenoid sources. *Food Chemistry, 272*(August 2018), 216–221. https://doi.org/10.1016/j.foodchem.2018.08.053

Olsmats, E., Ravindranathan, R. P., Knudsen, K. D., Kohlbrecher, J., Bonn, D., & Rennie, A. R. (2025). Emulsions stabilized by pea protein – Hydration and protein distribution. *Food Hydrocolloids, 162*, Article 110989. https://doi.org/10.1016/j.foodhyd.2024.110989

Olsmats, E., & Rennie, A. R. (2024). Understanding stabilization of oil-in-water emulsions with pea protein—studies of structure and properties. *Langmuir, 40*(26), 13386–13396. https://doi.org/10.1021/acs.langmuir.4c00540

Pereira, E., Ferreira, M. C., Sampaio, K. A., Grimaldi, R., Meirelles, A. J.d. A., & Maximo, G. J. (2019). Physical properties of Amazonian fats and oils and their blends. *Food Chemistry, 278*, 208–215. https://doi.org/10.1016/j.foodchem.2018.11.016

Peyronel, F., Cooney, J., Papp-Szabo, E., Martini, S., & Pink, D. (2023). X-ray characterization of three possible edible oleogelators: Experiment and theory. *Journal of the American Oil Chemists' Society, 100*(12), 961–974. https://doi.org/10.1002/aocs.12732

Pinna, N., Blasi, F., Ricci, M., & Schoubben, A. (2025). Influence of nanoencapsulation and freeze-drying on the antioxidant capacity of a carotenoid-rich extract from pumpkin. *Applied Food Research, 5*(1), Article 100799. https://doi.org/10.1016/j.afres.2025.100799

Plaha, N. S., Kaushik, N., Awasthi, S., Singh, M., Kaur, V., Langyan, S., … Kalia, S. (2023). Comparison of the nutritional quality of 14 wild Linum species based on fatty acid composition, lipid health indices, and chemometric approaches to unravel their nutraceutical potential. *Heliyon, 9*(11), Article e21192. https://doi.org/10.1016/j.heliyon.2023.e21192

Polińska, M., Rozanski, A., Galeski, A., & Bojda, J. (2021). The Modulus of the amorphous phase of Semicrystalline polymers. *Macromolecules, 54*(19), 9113–9123. https://doi.org/10.1021/acs.macromol.1c01576

Polmann, G., Teixeira, G. L., Santos, P. H., Rivera, G.Á., Ibañez, E., Cifuentes, A., … Block, J. M. (2024). Chemical characterization of gurguéia nut (*Dipteryx lacunifera* Ducke) and press cake oil obtained by hydraulic pressing and supercritical extraction. *Biomass Conversion and Biorefinery, 14*(16), 19065–19080. https://doi.org/10.1007/s13399-023-04042-x

Pommella, A., Mathonnat, M., & In, M. (2020). Texturing edible oil with crystals of phenolic compounds: Platelets versus rods. *Journal of Food Engineering, 283*, 110039. https://doi.org/10.1016/j.jfoodeng.2020.110039

Rajagukguk, Y. V., Islam, M., Grygier, A., & Tomaszewska-Gras, J. (2023). Thermal and spectroscopic profiles variation of cold-pressed raspberry seed oil studied by DSC, UV/VIS, and FTIR techniques. *Journal of Food Composition and Analysis, 124*, Article 105723. https://doi.org/10.1016/j.jfca.2023.105723

Rondou, K., Dewettinck, A., Dewettinck, K., & Van Bockstaele, F. (2024). Structural Build-Up and Stability of Hybrid Monoglyceride–Triglyceride Oleogels. *Gels, 10*(10), Article 650. https://doi.org/10.3390/gels10100650

Sadler, G., Davis, J., & Dezman, D. (1990). Rapid extraction of lycopene and β-carotene from reconstituted tomato paste and Pink grapefruit homogenates. *Journal of Food Science, 55*, 1460–1461. https://doi.org/10.1111/j.1365-2621.1990.tb03958.x

Saini, R. K., Prasad, P., Lokesh, V., Shang, X., Shin, J., Keum, Y.-S., & Lee, J.-H. (2022). Carotenoids: Dietary sources, extraction, encapsulation, bioavailability, and health benefits—A review of recent advancements. *Antioxidants, 11*(4), 795. https://doi.org/10.3390/antiox11040795

Santos, M.-K. M. S., Sousa, M. H., & Chaker, J. A. (2021). Drug dual-release matrix proprieties and the correlations with nanostructure aggregation kinetics for siloxane-polyether/hydrogel nanocomposites. *RSC Advances, 11*(7), 3863–3869. https://doi.org/10.1039/D0RA08270H

Schweiggert, R. M., Mezger, D., Schimpf, F., Steingass, C. B., & Carle, R. (2012). Influence of chromoplast morphology on carotenoid bioaccessibility of carrot, mango, papaya, and tomato. *Food Chemistry, 135*(4), 2736–2742. https://doi.org/10.1016/j.foodchem.2012.07.035

Silva, A. O., Sassi, G. R., Santos, M.-K. M. S., Oliveira, S. M. P. V., Gomide, G., Junior, V. F. V., … Sousa, M. H. (2024). Andiroba oil (*Carapa guianensis*) and ginger extract (*Zingiber officinale*)-loaded nanoemulsion: Elaboration, characterization, antioxidant activity, and cell viability investigation. *Colloids and Surfaces A: Physicochemical and Engineering Aspects, 702*, Article 134990. https://doi.org/10.1016/j.colsurfa.2024.134990

Sousa, H. M. S., Leal, G. F., da Silva Gualberto, L., de Freitas, B. C. B., Guarda, P. M., Borges, S. V., … de Souza Martins, G. A. (2025). Exploration of the chemical characteristics and bioactive and antioxidant potential of Tucumã (*Astrocaryum vulgare*), peach palm (*Bactris gasipaes*), and bacupari (*Garcinia gardneriana*), native Brazilian fruits. *Biomass Conversion and Biorefinery.*. https://doi.org/10.1007/s13399-023-05145-1

Taboada, N., Fernández Salom, M., Córdoba, A., González, S. N., López Alzogaray, S., & Van Nieuwenhove, C. (2022). Administration of a selected probiotic mixture improves body weight gain and the fatty acid composition of meat in creole goats. *Food Bioscience, 49*, Article 101836. https://doi.org/10.1016/j.fbio.2022.101836

Tian, M., Bai, Y., Tian, H., & Zhao, X. (2023). The chemical composition and health-promoting benefits of vegetable oils—A review. *Molecules, 28*(17), 6393. https://doi.org/10.3390/molecules28176393

Tomaszewska-Gras, J., Islam, M., Grzeca, L., Kaczmarek, A., & Fornal, E. (2021). Comprehensive thermal characteristics of different cultivars of flaxseed oil (Linum usittatissimum L.). *Molecules, 26*(7), Article 1958. https://doi.org/10.3390/molecules26071958

Wijngaard, H., Hossain, M. B., Rai, D. K., & Brunton, N. (2012). Techniques to extract bioactive compounds from food by-products of plant origin. *Food Research International, 46*(2), 505–513. https://doi.org/10.1016/j.foodres.2011.09.027

Zeb, A., & Murkovic, M. (2011). Carotenoids and triacylglycerols interactions during thermal oxidation of refined olive oil. *Food Chemistry, 127*(4), 1584–1593. https://doi.org/10.1016/j.foodchem.2011.02.022

Zhang, R., Lu, H., Wei, L., Lin, X., Yang, Z., Qi, J., & Zhang, Z. (2025). Self-Assembly at Oil–Water Interfaces Driven by Solubility Differences and Polar–Hydrophobic Interactions: An Insight into a Highly Mechanical Performance Gel with Gradients. *Langmuir, 41*(16), 10305–10314. https://doi.org/10.1021/acs.langmuir.5c00131

International Olive Council [IOC] (2017). Determination of Fatty Acid Methyl Esters by Gas Chromatography., COI/T.20/Doc. No 33. International Olive Council, [IOC] https://www.internationaloliveoil.org/wp-content/uploads/2023/11/COI-T20-33-rev-1-ENG.pdf.